Chinese Chemical Letters 36 (2025) 110248

Contents lists available at ScienceDirect

Chinese Chemical Letters

journal homepage: www.elsevier.com/locate/cclet

A luminescent folded S-shaped high-nuclearity Eu_{19}-oxo-cluster embedded polyoxoniobate for information encryption

Wen-Jun Xia, Yong-Jiang Wang, Yun-Fei Cao, Cai Sun, Xin-Xiong Li, Yan-Qiong Sun*, Shou-Tian Zheng*

College of Chemistry, Fuzhou University, Fuzhou 350108, China

ARTICLE INFO

Article history:
Received 5 June 2024
Revised 25 June 2024
Accepted 12 July 2024
Available online 14 July 2024

Keywords:
Polyoxoniobate
Lanthanide
Luminescence
Information encryption
Acid/alkali stimulation

ABSTRACT

Ln-containing polyoxoniobates (PONbs) have appealing applications in luminescence, information encryption and magnetic fields, but the synthesis of PONbs containing high-nuclearity Ln-O clusters is challenging due to the easy hydrolysis of Ln^{3+} ions in alkaline environments. In this paper, we are able to integrate CO_3^{2-} and high-nuclearity Ln-O clusters into PONb to construct an inorganic giant Eu_{19}-embedded PONb $H_{49}K_{16}Na_{13}(H_2O)_{63}[Eu_{21}O_2(OH)_7(H_2O)_5(Nb_7O_{22})_{10}(Nb_2O_6)_2(CO_3)_{18}]\cdot 91H_2O$ (**1**), which contains the highest nuclearity Eu-O clusters and the largest number of Eu^{3+} ions among PONbs. In addition, the film that was prepared by mixing **1** with gelatin and glycerol, exhibits reversible luminescence switching behavior under acid/alkali stimulation and has been used to create a fluorescence-encoded information approach. This work paves a feasible strategy for the construction of high-nuclearity Ln-O cluster-containing PONbs and the expansion of the application of Ln-containing PONbs in information encryption.

Information security is of great importance to people's lives, social stability, and even national security, which promotes the development of anti-counterfeiting materials and effective information encryption/decryption strategies [1-5]. Fluorescent materials with high plasticity and excellent optical performance have been the ideal optical anti-counterfeiting materials pursued by people. The fluorescent anti-counterfeiting technology in optical anti-counterfeiting has been of great interest to researchers due to its advantages of high stability, fast information extraction, and strong concealment [6-10]. Therefore, it is crucial to select suitable fluorescent anti-counterfeiting materials. Currently, a lot of fluorescent materials are synthesized using organic chromophores, which are expensive, difficult to synthesize, and have certain toxicity drawbacks [11-13]. In contrast, lanthanide-based luminescent materials have attracted much attention due to their large Stokes, long fluorescence lifetime, and narrow emission in the visible and near-infrared regions [14,15]. However, the luminescence is unsatisfactory due to the forbidden 4f-4f jump of the lanthanide ions [16]. Polyoxometalates (POMs) have attracted considerable attention from researchers in recent years due to their ability to sensitize the luminescence of lanthanide ions [17].

As an important branch in the field of polyoxometalates (POMs) [18-21], polyoxoniobates (PONbs) are still at a preliminary stage of exploration compared to the current research and maturity of polyoxomolybdates [22], polyoxotungstates [23-25], and polyoxovanadates [26]. PONbs can be classified into two categories: Isopolyoxoniobates (iso-PONbs) and heteropolyoxoniobates (hetero-PONbs). Since Lindqvist reported the first case of PONb $\{Nb_6O_{19}\}$ in 1953 [27], $\{Nb_6O_{19}\}$ has been found to have excellent binding ability as a precursor in aqueous solution. Iso-PONbs such as $\{Nb_{10}O_{28}\}$ [28], $\{Nb_{24}O_{72}\}$ [29], $\{Nb_{52}O_{150}\}$ [30], $\{Nb_{288}O_{768}(OH)_{48}(CO_3)_{12}\}$ [31], have been successively prepared. In recent years, the introduction of transition metal ions into PONb systems to produce hetero-PONbs has been reported. These include $\{Co_{33}Nb_{54}\}$ [32], $\{Co_{26}Nb_{36}\}$ [33], $\{Cu_{25.5}Nb_{56}\}$ [34], $\{Ni_{10}Nb_{32}\}$ [35], and $\{Fe_{10}Nb_{48}\}$ [36]. In the field of lanthanide-containing hetero-PONbs, it is difficult to introduce lanthanide ions with excellent optical [37], magnetic [38], and catalytic [39,40] properties into PONb systems because the solubility of Ln^{3+} cations is inhibited under the reaction conditions of PONbs (usually pH > 10) [34]. However, POMs containing Ln-oxo clusters are mostly found in polyoxotungstate systems, such as $\{Ln_{27}Ge_{10}W_{106}O_{406}(OH)_4(H_2O)_{24}\}$ (Ln = La and Ce) [41], $\{Ln_{30}Ge_{12}W_{107}O_{420}(OH)_2(H_2O)_{14}\}$ (Ln = Eu and Sm) [42]. In contrast to polyoxotungstates containing high-nuclearity Ln-oxo clusters, the PONbs containing Ln-oxo clusters are still rare and contain fewer Ln^{3+} ions. Using the strategy of oxalate syner-

* Corresponding authors.
E-mail addresses: sunyq@fzu.edu.cn (Y.-Q. Sun), stzheng@fzu.edu.cn (S.-T. Zheng).

https://doi.org/10.1016/j.cclet.2024.110248
1001-8417/

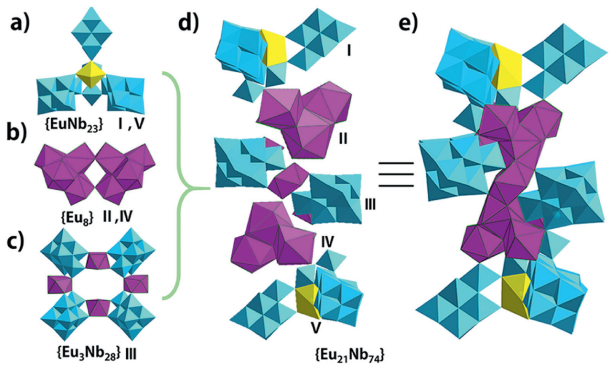

Fig. 1. Schematic diagram assembly of {**Eu$_{21}$Nb$_{74}$**} cluster in **1**: (a) {**EuNb$_{23}$**} cluster; (b) {**Eu$_8$**} unit; (c) {**Eu$_3$Nb$_{28}$**} cluster. (d) Five-layered structure in {**Eu$_{21}$Nb$_{74}$**} cluster; (e) {**Eu$_{21}$Nb$_{74}$**} cluster. Polyhedral key: NbO_6, cyan; EuO_n ($n = 7$, 8, 9, 10), purple-red/yellow.

gistic coordination, our group has for the first time obtained a lanthanide-containing PONb {$Dy_{14}Nb_{192}$} [43], which contains the highest number of Ln^{3+} ions to date. However, there are no high-nuclearity Ln-oxo clusters in {$Dy_{14}Nb_{192}$}. In 2023, a series of hexa-nuclear {$Ln_6(\mu_3\text{-}OH)_6$} cluster encapsulated polyoxoniobate {$Ln_6(\mu_3\text{-}OH)_6(SiNb_{18}O_{54})_3$} was synthesized in the presence of Cu^{2+} and ethylenediamine [44]. A polyoxoniobate {$Dy_4(RA)_2Nb_{32}$}$_2$ (RA = risedronic acid) containing tetranuclear Ln-oxo clusters has been obtained using organophosphonic acid ligands [45]. Thus, there are still significant gaps in the synthesis of lanthanide-containing PONbs. It is an attractive challenge to prepare high-nuclearity Ln-oxo clusters incorporated PONbs.

In this paper, we report an all-inorganic S-shaped high-nuclearity Eu_{19}-oxo-clusters embedded polyoxoniobate $H_{49}K_{16}Na_{13}(H_2O)_{63}[Eu_{21}O_2(OH)_7(H_2O)_5(Nb_7O_{22})_{10}(Nb_2O_6)_2(CO_3)_{18}]\cdot 91H_2O$ (**1**). The polyanion {$Eu_{21}O_2(OH)_7(H_2O)_5$}{$(Nb_7O_{22})_{10}(Nb_2O_6)_2(CO_3)_{18}$} ({**Eu$_{21}Nb_{74}$**}) in **1** has a giant hamburger-like five-layered sandwich structure (Fig. 1). Compound **1** was used to prepare a thin film by mixing it with gelatin and glycerol, and the film exhibited reversible luminescence switching behavior in the presence of acid/alkali. Based on this property, the film is used in the field of acid/alkali cross-stimulated fluorescence encryption materials.

Compound **1** crystallizes in the triclinic space group *P*-1 and contains a centrosymmetric polyanion cluster {**Eu$_{21}$Nb$_{74}$**} (Fig. 1e), as well as K^+ and Na^+ cations. The {**Eu$_{21}$Nb$_{74}$**} polyanion has a five-layered sandwich structure. It contains two new pinwheel-shaped clusters {$EuO_2(Nb_2O_6)(Nb_7O_{22})_3$} ({$EuNb_{23}$} as top and bottom layers, one {$Eu_3O_6(Nb_7O_{22})_4$}({Eu_3Nb_{28}}) cluster as a middle layer and two octanuclear {$Eu_8O_4(CO_3)_9$} ({Eu_8}) clusters as filler layers (Fig. 1d).

The top and bottom layers are two centrosymmetric {$EuNb_{23}$} fragments (Fig. 1a). Two NbO_6 octahedra are bridged *via* vertex-sharing to form a dinuclear {Nb_2O_6} cluster. Three {Nb_7O_{22}} ({Nb_7}) subunits are arranged around the dinuclear {Nb_2O_6} fragment, generating an intriguing pinwheel-shaped {$(Nb_2O_6)(Nb_7O_{22})_3$} ({Nb_{23}}) cluster (Fig. S1a in Supporting information). The arrangement of the three {Nb_7} cluster units can be represented as an approximate equilateral triangle. The {Nb_7} cluster units are located on each of its three vertices (approximately 10.552 Å × 10.417 Å × 9.995 Å in size). The angles of the triangle are close to 60° (Fig. S1b in Supporting information). Unlike the reported V-shaped {Nb_{23}} [46], the pinwheel-shaped {Nb_{23}} motif represents a new type of PONb subunit in the PONb family (Fig. S2 in Supporting information). At the same time, an EuO_8 dodecahedron is capped on the center of the {Nb_{23}} fragment to form a pinwheel-shaped lanthanide-incorporated {$EuNb_{23}$}. The eight-coordinated Eu^{3+} is coordinated by six O atoms from the three {Nb_7} units, and two terminal water molecules (Fig. S1c in Supporting information).

The middle layer is a centrosymmetric square {Eu_3Nb_{28}} motif (Fig. 1c). In the {Eu_3Nb_{28}}, there are two equivalent 0.5 occupied Eu atoms. The Eu atom splits into two Eu atoms with occupancies of 0.4 for Eu3 and 0.1 for Eu3A (Fig. S2 in Supporting information), indicating that 0.5 Ln^{3+} is disorderly occupied in two positions. The centrosymmetric {Eu_3Nb_{28}} is composed of four EuO_8 polyhedrons and four {Nb_7O_{22}} units linked by vertex-sharing to form a square lanthanide-encapsulated PONb cluster, similar to the known {α-$Nb_{32}O_{96}$} (Fig. S3b in Supporting information) [29]. The difference is that in the {Eu_3Nb_{28}} subunit, the EuO_8 polyhedrons replace the four {NbO_6} octahedra in the classical {α-Nb_{32}} subunit. The {Eu_3Nb_{28}} consists of a heterometallic {Eu_3Nb_4} 8-ring linking four Lindqvist {Nb_6O_{19}} clusters *via* Eu-O-Nb and Nb-O-Nb bonds. The arrangement of the four EuO_8 polyhedrons can be described as a rhombus with the EuO_8 units located at each of the four vertices of the rhombus. The distance between two neighbouring Eu atoms is 7.4 Å (Fig. S3a in Supporting information). These four Eu atoms adopt 8-coordinated tetragonal antiprismatic geometries. The four {Nb_6O_{19}} clusters are symmetrically arranged on either sides of the {Eu_3Nb_4} 8-ring plane, forming a centrosymmetric square lanthanide-encapsulated PONb cluster. It is unusual in the PONb system that Eu and Nb atoms are alternately arranged to form a square lanthanide-incorporated PONb.

The filler layers between the top layer and middle layers, as well as between the bottom layer and middle layers, are composed of {Eu_8} lanthanide-oxo clusters. The inorganic CO_3^{2-} ligands act as linkers and anionic templates between the Eu^{3+} cations, giving rise to a pair of Eu_8 octanuclear lanthanide clusters, each of which contains two tetranuclear tetrahedron-shaped {$Eu_4O_2(CO_3)_4$} ({Eu_4}) clusters (Fig. 1b and Fig. S4 in Supporting information). The four CO_3^{2-} anions bridge four Eu atoms *via* μ_2-O or μ_3-O of the CO_3^{2-} anions to form a tetrahedron-shaped {Eu_4} cluster with the CO_3^{2-} anions situated on the edges of the {Eu_4} tetrahedron (Fig. S4a). The two {Eu_4} clusters are connected by one CO_3^{2-} and two μ_2-O atoms, resulting in an {Eu_8} cluster. There are four types of coordination geometries in the {Eu_8}: EuO_7 mono-capped trigonal prism, EuO_8 dodecahedron, EuO_9 mono-capped square antiprism and EuO_{10} bicapped square antiprism (Fig. S5 in Supporting information). The two {Eu_8} clusters are orthogonally capped above and below the square plane defined by four Eu^{3+} ions from the middle layer {Eu_3Nb_{28}}. Each {Eu_8} cluster is connected to three Eu^{3+} cations and two Nb atoms by Eu–O–Eu and Nb–O–Eu bonds. At the same time, the two {Eu_8} clusters are connected to {$EuNb_{23}$} fragments from the top and bottom layers by {Nb_2O_6} clusters, respectively, giving rise to a giant lanthanide-oxo-cluster-embedded sandwich PONb cluster {$Eu_{21}Nb_{74}$}.

The most striking feature of {$Eu_{21}Nb_{74}$} is the presence of a folded "S"-shaped 19-nuclear {$Eu_{19}O_{93}(OH)_5(H_2O)_3$}({$Eu_{19}$}) wheel cluster (Fig. 2a), which is the highest-nuclearity lanthanide-oxo cluster found in the PONbs system. In {Eu_{19}}, ten EuO_n ($n = 7$, 8, 9, 10) polyhedrons are edge- or face-shared to form an {Eu_9} wheel cluster and two T-shaped {Eu_5} clusters are symmetrically distributed on the top and bottom of the {Eu_9} plane, resulting in a folded "S"-shaped 19-nuclear {Eu_{19}} cluster (Figs. 2b and c). Two {EuO_8} dodecahedrons of two {$EuNb_{23}$} are connected to the {Eu_{19}} cluster by {Nb_2O_6} clusters to form an {$Eu_{21}Nb_4$} nanocluster.

More interestingly, the polyanion {**Eu$_{21}$Nb$_{74}$**} clusters can be described as a high-nuclearity Eu_{19}-oxo-clusters embedded polyoxoniobate, in which the heterometal-oxo {$Eu_{21}Nb_4$} nanocluster is encapsulated by ten {Nb_7} clusters. The arrangement of the ten {Nb_7} clusters can be viewed as a distorted pentagonal antiprism with ten {Nb_7} clusters at the vertices (Fig. 2d). The {Nb_7} clusters are good inorganic ligands and can easily coordinate with the inner Eu^{3+} cations. Interestingly, the charge of the polyanion

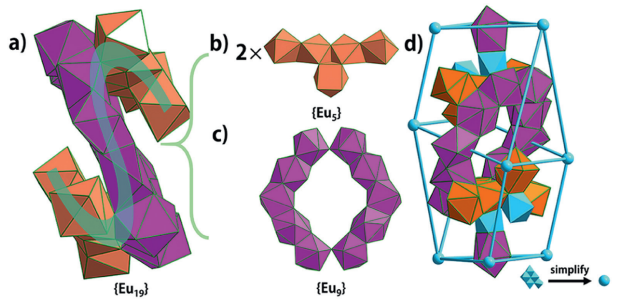

Fig. 2. (a) Polyhedral representation of the folded "S"-shaped {**Eu$_{19}$**} cluster. (b) T-shaped {Eu_5} cluster. (c) Wheel cluster. (d) The simplified structure diagram of {**Eu$_{21}$Nb$_{74}$**} cluster. Polyhedral key: NbO_6, cyan; EuO_n ($n = 7$, 8, 9, 10), purple-red/orange.

in {**Eu$_{21}$Nb$_{74}$**} is balanced by K^+ and Na^+ cations, which fill the empty spaces of the {**Eu$_{21}$Nb$_{74}$**} cluster and bind to CO_3^{2-}. There are two K^+ cations located in the center of the {Eu_9} wheel cluster (Fig. S6 in Supporting information). To the best of our knowledge, such an inorganic PONb containing a high-nuclearity lanthanide-oxo-cluster has not been reported to date.

Europium compounds have been extensively investigated due to their stable emission, long lifetime, and narrow emission bandwidth [16]. Therefore, the introduction of Eu^{3+} ions into PONb clusters can impart unique luminescence properties. The process and mechanism of energy transfer from polyoxoniobate to Eu^{3+} ions, resulting in the sensitized emission of Eu^{3+} in PONbs, has been reported in the literature [17,47,48]. This emission arises from the O → Nb triplet state *via* the singlet state, with a Förster-Dexter dipole-dipole coupling between the donor and the acceptor. Compound **1** displays intense red luminescence and four characteristic luminescence peaks of Eu^{3+} at 591, 614, 650, and 702 nm are observed under 395 nm excitation, which are attributed to the $^5D_0 \rightarrow {}^7F_1$, $^5D_0 \rightarrow {}^7F_2$, $^5D_0 \rightarrow {}^7F_3$ and $^5D_0 \rightarrow {}^7F_4$ transitions (Fig. S7 in Supporting information). Furthermore, the $^5D_0 \rightarrow {}^7F_2$ transition of the electric dipole is influenced by the ligand environment of Eu^{3+} and is highly sensitive to local changes. Conversely, the $^5D_0 \rightarrow {}^7F_1$ transition of the magnetic dipole is less sensitive to environmental variations. The fluorescence lifetime curve of **1** was tested based on its strongest characteristic emission peak (614 nm) and excitation peak (395 nm) (Fig. S8 in Supporting information). The fluorescence lifetime of **1** was determined by fitting the lifetime curve with a monoexponential function $I = A\exp(-t/\tau)$, where τ is the lifetime and A is the pre-exponential factor. The obtained value for τ is 372 μs and A is 1.24, and the lifetime of 1 is very long, indicating that the PONb clusters can sensitize the Eu(III) emission to the large extent.

As nanoscale clusters with a well-defined atomic structure, PONbs possess rich structures [49]. Crucially, PONbs are excellent inorganic ligands for sensitizing the luminescence of Eu^{3+}. However, PONbs are poorly dispersed and have few practical applications. It is worth mentioning that the combination of the polymer gelatin, which is malleable, non-toxic, and low-cost, with PONbs can improve the processability of polyoxometalates.

Gelatin/**1**/GL films were easily obtained by adding an appropriate amount of **1** aqueous solution into gelatin and glycerol (GL). ATR FTIR was used to characterize gelatin/1 mixed systems (Fig. S9a in Supporting information). The characteristic peaks of **1** in Gelatin/$1_{20\ mg}$ at 1031 cm^{-1} and 864 cm^{-1} are attributed to ν(Nb=Od), and ν(Nb-Ob-Nb) respectively. These results indicate that 1 is dispersed in a gelatin matrix and maintain an intact structure. According to the EDS results, the film was found to contain Eu and Nb atoms, thus {$Eu_{21}Nb_{74}$} clusters were found to be uniformly dispersed in the film (Figs. S9b-d in Supporting information). The mechanical properties of the Gelatin/**1** film were poor. However, the flexibility of the film was improved by the addition of GL. GL can improve the fluidity of the material by reducing the intermolecular forces, giving the film excellent flexibility [44].

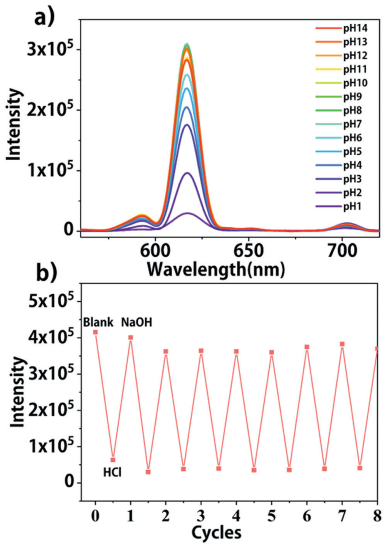

Fig. 3. (a) The luminescence of Gelatin$_{0.2\ g}$/**1**$_{20\ mg}$/GL$_{150\ \mu L}$ films under different pH conditions. (b) Recycling detection tests of Gelatin/**1**$_{20\ mg}$/GL$_{150\ \mu L}$ film with 8 times.

As shown in Fig. S10 (Supporting information), the fluorescence emission spectra of the films were measured under excitation at a wavelength of 267 nm (Fig. S11 in Supporting information). In addition, the luminescence intensity of the films is influenced by the content of GL and **1**, respectively. When the GL content is gradually increased in the range of 0–350 μL, the luminescence intensity of the films is the strongest at the content of 150 μL. The fluorescence lifetimes of the films were measured under a series of conditions with different GL contents, and it was found that the fluorescence lifetimes of the films remained unchanged (Fig. S12 in Supporting information). When the content of **1** is increased in the range of 5–40 mg, the luminescence intensity of the film is close to the maximum at the content of 20 mg (Fig. S10a). Meanwhile, the fluorescence lifetimes of the films of sample **1** with different contents were examined, and we observed that the fluorescence lifetimes of the films remained unchanged (Fig. S13 in Supporting information). Therefore, the Gelatin$_{0.2\ g}$/**1**$_{20\ mg}$/GL$_{150\ \mu L}$ film is the most suitable for studying the information encryption function.

Gelatin$_{0.2\ g}$/**1**$_{20\ mg}$/GL$_{150\ \mu L}$ film exhibits reversible luminescence and fluorescence quenching transition phenomena under HCl/NaOH stimulation. The characteristic emission peaks of gelatin$_{0.2\ g}$/**1**$_{20\ mg}$/GL$_{150\ \mu L}$ film show a decreasing trend with decreasing pH in the acidic environment (Fig. 3a). However, in the alkaline environment, the intensity of the characteristic emission peaks of the films remains essentially unchanged with increasing pH (Fig. 3a). It is well known that Eu-PONbs exhibit red fluorescence under UV irradiation due to the intramolecular energy transfer from the PONbs to Eu^{3+}, which can be divided into two steps [17,47,48]. First, the photo-excitation of the O → Nb LMCT leads to the hopping of the d^1 electron, accompanied by energy release through deactivated recombination between the d^1 electron and the hole. Second, the energy transfer from the O → Nb LMCT state to the $^5D_0$ emission state of the Eu^{3+} ion in the lattice stimulates the emission of Eu^{3+}. The emission originates from the $^5D_0$ excited state. It is interesting to note that the luminescence of the Gelatin$_{0.2\ g}$/**1**$_{20\ mg}$/GL$_{150\ \mu L}$ film is almost quenched at the pH values below 1. However, the luminescence is gradually enhanced as the pH values increase from 1 to 12. A slow decrease in lumines-

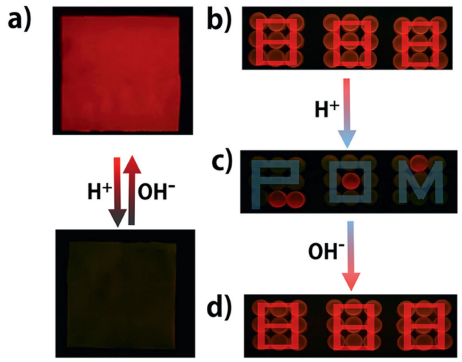

Fig. 4. (a) Images of luminescent switching behavior of Gelatin/$\mathbf{1}_{20\ mg}$/$GL_{150\ \mu L}$ hydrogel upon HCl/NaOH stimuli. (b) Cylindrical gel combination showed "888" pattern. (c) Cylindrical gel combination showed "POM" pattern after HCl treatment. (d) Cylindrical gel restored luminescence after NaOH treatment.

cence intensity is observed as the pH increases from 13 to 14, due to the formation of $Eu(OH)_3$ precipitates.

How does H^+ affect the luminescence properties of $Gelatin_{0.2\ g}$/$\mathbf{1}_{20\ mg}$/$GL_{150\ \mu L}$ film? When the polymeric gelatin and glycerol are used to make the $Gelatin_{0.2\ g}$/$\mathbf{1}_{20\ mg}$/$GL_{150\ \mu L}$ film, the hydrogen bonds are formed between the O–H groups and the O atoms of NbO_6 [50,51]. When hydrochloric acid is sprayed on the $Gelatin_{0.2\ g}$/$\mathbf{1}_{20\ mg}$/$GL_{150\ \mu L}$ film, the hydrogen bonds between the O–H groups and NbO_6 are protonated, preventing the above second step, *i.e.*, the energy transfer from the O → Nb LMCT state to the $^5D_0$ emission state of the Eu^{3+} ion (Fig. S14 in Supporting information). Therefore, the luminescence intensity of the acid-treated film is weakened. The fluorescence lifetime of the acid-treated films was also investigated and showed a decrease from 385 μs to 280 μs (Fig. S15 in Supporting information). When the film is immersed in 0.5 mol/L NaOH solution, the H^+ ions that act as bridges between O–H groups and NbO_6 are neutralized by OH^-, causing the hydrogen atom to be hydrogen-bonded with the NbO_6, which does not affect the energy transfer from O →Nb LMCT states to the Eu(III) cation. Therefore, the characteristic red emission color of the $Gelatin_{0.2\ g}$/$\mathbf{1}_{20\ mg}$/$GL_{150\ \mu L}$ film is recovered. Under 254 nm UV irradiation, the corresponding change in luminescence intensity can be clearly observed (Fig. 4a). This is consistent with the recovery of the luminescence lifetime (Fig. S16 in Supporting information).

Molten $gelatin_{0.2\ g}$/$\mathbf{1}_{20\ mg}$/$GL_{150\ \mu L}$ was poured into a cylindrical mold and dried for 6 h before removal. The "888" red light pattern formed by the combination of the molds is observed under the 254 nm UV light (Fig. 4b). Based on the "888" pattern, we attenuated the fluorescence of a portion of the cylindrical gel by adding hydrochloric acid solution drop by drop to display the real information "POM" (Fig. 4c). The luminescence ability of the gel can be restored by subsequent immersion of the cylindrical gel in 0.5 mol/L NaOH solution (Fig. 4d). The cyclic stability of the gel was also tested and found to be capable of performing eight cycles of luminescence switching behaviour (Fig. 3b). The result indicates that the gel exhibits excellent cyclic stability. This provides a prerequisite for the reversible input and erasure of encrypted information and demonstrates the potential of the film material as an encryption material.

In conclusion, the first high-nuclearity lanthanide-oxo-cluster embedded polyoxoniobate with a huge five-layered sandwich structure has been constructed from pinwheel-shaped $\{EuNb_{23}\}$, square lanthanide-incorporated PONb cluster $\{Eu_3Nb_{28}\}$ and octanuclear $\{Eu_8\}$ clusters. The CO_3^{2-} plays a key role in the self-assembly of Ln^{3+} cations into clusters. Such $\{\mathbf{Eu_{21}Nb_{74}}\}$ clusters can be described as a folded S-shaped high-nuclearity Eu_{19}-oxo-cluster embedded polyoxoniobate. To the best of our knowledge, compound **1** contains highest-nuclearity Ln-O cluster and the largest number of Ln in PONbs and represents a new type of unusual structure of Ln-containing PONbs. Compound **1** is mixed with gelatin and glycerol to form a film, and the film exhibits reversible luminescence switching behavior under acid/alkali stimulation. The reversible luminescence switching behavior under acid/alkali stimulation enables encrypted information. This study demonstrates a feasible self-assembly strategy for PONb systems containing high-nuclearity Ln-O clusters, and also provides a direction for exploring the properties of Eu-PONb clusters.

Declaration of competing interest

The authors declare that we do not have any commercial or associative interest that represents a conflict of interest in connection with the work submitted.

CRediT authorship contribution statement

Wen-Jun Xia: Writing – original draft, Investigation, Data curation. **Yong-Jiang Wang:** Investigation, Data curation. **Yun-Fei Cao:** Software, Data curation. **Cai Sun:** Software, Funding acquisition, Conceptualization. **Xin-Xiong Li:** Software, Funding acquisition, Conceptualization. **Yan-Qiong Sun:** Writing – review & editing, Project administration, Funding acquisition. **Shou-Tian Zheng:** Project administration, Funding acquisition, Conceptualization.

Acknowledgment

We gratefully acknowledge the financial support from the National Natural Science Foundation of China (Nos. 21971040, 22171045, and 22371046).

Supplementary materials

Supplementary material associated with this article can be found, in the online version, at doi:10.1016/j.cclet.2024.110248.

References

[1] R. Arppe, T.J. Sorensen, Nat. Rev. Chem. 1 (2017) 0031.
[2] L.E. MacKenzie, R. Pal, Nat. Rev. Chem. 5 (2021) 109–124.
[3] Z.Y. Quan, Q. Zhang, H.J. Li, et al., Coord. Chem. Rev. 493 (2023) 215287.
[4] Y. Shen, X. Le, Y. Wu, et al., Chem. Soc. Rev. 53 (2024) 606–623.
[5] Y. Sun, X.X. Le, S.Y. Zhou, et al., Adv. Mater. 34 (2022) 2201262.
[6] C.W. Liu, A.K. Steppert, Y.Z. Liu, et al., Adv. Mater. 35 (2023) 2303120.
[7] H.W. Huang, H.T. Li, J.M. Yin, et al., Adv. Mater. 35 (2023) 2211117.
[8] Y. Li, J. Sun, M. Chen, et al., Adv. Funct. Mater. 32 (2022) 2205494.
[9] Z.C. Zeng, B.L. Huang, X. Wang, et al., Adv. Mater. 32 (2020) 2004506.
[10] L.J. Ding, X.D. Wang, J. Am. Chem. Soc. 142 (2020) 13558–13564.
[11] H.Q. Zheng, Y. Yang, Z.Y. Wang, et al., Adv. Mater. 35 (2023) 2300177.
[12] R. Xiaotian, W. Ota, T. Sato, et al., Angew. Chem. Int. Ed. 62 (2023) e202302550.
[13] H. Xu, Z. Zhang, L. Huang, et al., Chem. Eng. J. 450 (2022) 138458.
[14] W. Chen, R.Q. Fan, H.J. Zhang, et al., Dalton Trans. 46 (2017) 4265–4277.
[15] J.C.G. Bünzli, Eur. J. Inorg. Chem. 2017 (2017) 5058–5063.
[16] S.V. Eliseeva, J.C.G. Bünzli, Chem. Soc. Rev. 39 (2010) 189–227.
[17] T. Yamase, Chem. Rev. 98 (1998) 307–325.
[18] D.L. Long, R. Tsunashima, L. Cronin, Angew. Chem. Int. Ed. 49 (2010) 1736–1758.
[19] Z. Zeb, Y. Huang, L. Chen, et al., Coord. Chem. Rev. 482 (2023) 215058.
[20] Y. Zhang, Y. Liu, D. Wang, et al., Polyoxometalates 2 (2023) 9140017.
[21] Y. Tai, W. Sun, D. Yao, et al., Polyoxometalates 3 (2024) 9140051.
[22] D.H. Li, X.Y. Zhang, J.Q. Lv, et al., Angew. Chem. Int. Ed. 62 (2023) e202312706.
[23] H.P. Xiao, Y.S. Hao, X.X. Li, et al., Angew. Chem. Int. Ed. 61 (2022) e202210019.
[24] N. Song, M. Lu, J. Liu, et al., Angew. Chem. Int. Ed. 63 (2024) e202319700.
[25] X. Liu, L. Cui, J. Jiang, et al., Chin. Chem. Lett. 33 (2022) 2630–2634.
[26] M. Aureliano, N.I. Gumerova, G. Sciortino, et al., Coord. Chem. Rev. 447 (2021) 214143.
[27] I. Lindqvist, Ark. Kemi. 5 (1953) 247–250.
[28] L. Shen, C.H. Li, Y.N. Chi, et al., Inorg. Chem. Commun. 11 (2008) 992–994.
[29] P. Huang, C. Qin, Z.M. Su, et al., J. Am. Chem. Soc. 134 (2012) 14004–14010.
[30] L. Jin, Z.K. Zhu, Y.L. Wu, et al., Angew. Chem. Int. Ed. 56 (2017) 16288–16292.
[31] Y.L. Wu, X.X. Li, Y.J. Qi, et al., Angew. Chem. Int. Ed. 57 (2018) 8572–8576.

[32] Z.W. Guo, L.H. Lin, J.P. Ye, et al., Angew. Chem. Int. Ed. 62 (2023) e202305260.
[33] Z.-W. Guo, Y. Chen, Z.-H. Chen, et al., Chin. Chem. Lett. 35 (2024) 109124.
[34] J.Y. Niu, P.T. Ma, H.Y. Niu, et al., Chem. Eur. J. 13 (2007) 8739–8748.
[35] Z.J. Liang, D.D. Zhang, H.Y. Wang, et al., Dalton Trans. 45 (2016) 16173–16176.
[36] M. Baranov, L. Polin, N. Leffler, et al., Dalton Trans. 51 (2022) 8600–8604.
[37] S. Yang, T.T. Gong, Y.C. Dai, et al., Inorg. Chem. 62 (2023) 17861–17869.
[38] Y.J. Wang, S.Y. Wu, Y.Q. Sun, et al., Chem. Commun. 55 (2019) 2857–2860.
[39] H.Y. Zhao, Y.Z. Li, J.W. Zhao, et al., Coord. Chem. Rev. 443 (2021) 213966.
[40] Y.F. Liu, C.W. Hu, G.P. Yang, Chin. Chem. Lett. 34 (2023) 108097.
[41] Z. Li, X.X. Li, T. Yang, et al., Angew. Chem. Int. Ed. 56 (2017) 2664–2669.
[42] Z. Li, Z.H. Lv, H. Yu, et al., CCS Chem. 4 (2022) 2938–2945.
[43] R.D. Lai, J. Zhang, X.X. Li, et al., J. Am. Chem. Soc. 144 (2022) 19603–19610.
[44] Z.K. Zhu, Y.Y. Lin, R.D. Lai, et al., Chin. Chem. Lett. 34 (2023) 107773.
[45] H. Yu, Y.D. Lin, S.L. Huang, et al., Angew. Chem. Int. Ed. 62 (2023) e202302111.
[46] H. Yu, Y.D. Lin, Z.Y. Liu, et al., Inorg. Chem. 61 (2022) 8112–8116.
[47] T. Yamase, Handb. Phys. Chem. Rare Earths 39 (2009) 297–356.
[48] Z. Yang, B. Yan, X. Li, et al., Inorg. Chem. 61 (2022) 12181–12189.
[49] J. Zhang, L.N. Wang, X.F. Chen, et al., Acta Phys. Chim Sin. 36 (2020) 1912002.
[50] Y.X. Guo, Y.J. Gong, Y.A. Gao, et al., Langmuir 32 (2016) 9293–9300.
[51] J. Yang, M. Chen, P. Li, et al., Sens. Actuator. B 273 (2018) 153–158.